Journal of Catalysis **200,** 259–269 (2001)
doi:10.1006/jcat.2001.3219, available online at http://www.idealibrary.com on IDEAL®

Catalytic Performance of the New Delaminated ITQ-2 Zeolite for Mild Hydrocracking and Aromatic Hydrogenation Processes

A. Corma,*[,1] A. Martínez,* and V. Martínez-Soria†

*Instituto de Tecnología Química UPV-CSIC, Avenida de los Naranjos s/n. 46022, Valencia, Spain; and †Departamento de Ingeniería Química, Universitat de València, 46100 Burjassot, Spain

Received September 12, 2000; revised December 15, 2000; accepted March 7, 2001; published online May 16, 2001

Catalysts based on NiMo and Pt supported on the new delaminated ITQ-2 zeolite have been prepared and their catalytic properties evaluated for the mild hydrocracking (MHC) of vacuum gasoil and aromatic hydrogenation. The results were compared with those obtained using other conventional supports, e.g., silica, γ-alumina, amorphous silica–alumina (25 wt% Al_2O_3), and USY zeolite, all of which contain the same metal loading as the ITQ-2 material. In the case of MHC of vacuum gasoil, NiMo/ITQ-2 displayed a higher hydrocracking activity than NiMo/SiO_2–Al_2O_3 and NiMo/γ-Al_2O_3, and even higher activity than NiMo/USY in the range 375–425°C. Moreover, NiMo/ITQ-2 had a selectivity to middle distillates intermediate between those of NiMo/USY and NiMo/SiO_2–Al_2O_3. For hydrogenation of naphthalene, Pt/ITQ-2 displayed higher activity than Pt/γ-Al_2O_3 and Pt/SiO_2-Al_2O_3 but lower activity than Pt/USY with similar Pt dispersion. This is explained by considering that some of the Pt centers located in the 10 MR channels of ITQ-2 are not accessible to the naphthalene molecules. Indeed, Pt/ITQ-2 is significantly more active than Pt/USY for the hydrogenation of benzene, which can access the metal sites in the 10 MR channels of the delaminated ITQ-2 zeolite. Furthermore, Pt/ITQ-2 gave the highest aromatic reduction when using a hydrotreated light cycle oil (HT-LCO) feedstock containing ca. 70 vol% total aromatics, 0.40 wt% S, and 480 ppm N. In this case, the larger external surface area of ITQ-2 as compared with USY may favor the hydrogenation of the voluminous aromatic molecules present in the HT-LCO feed. These results can be explained by the peculiar structure of the delaminated ITQ-2 zeolite, which combines the good activity of zeolites with the desired selectivity of amorphous catalysts, while minimizing the diffusional problems often encountered in microporous materials.

Key Words: **hydrocracking; aromatics hydrogenation; sulfur resistance; delaminated zeolite; ITQ-2; NiMo; platinum; supported catalysts.**

1. INTRODUCTION

The growing demand for middle distillates, together with the tighter specifications directed toward minimizing the environmental impact of automotive fuels, has increased the importance of hydrotreating processes in modern refinery schemes (1, 2). In particular, hydrogenation of aromatic-rich fractions and hydrocracking of heavy feedstocks are considered to be key processes in producing high-quality diesel fuels.

Mild hydrocracking (MHC) can be considered as an intermediate process between hydrotreating and conventional hydrocracking, and is typically used to convert heavy fractions, such as vacuum gasoil, into low-sulfur fuel oil and middle distillates of medium quality. MHC is performed at much lower hydrogen pressures (<5.0 MPa) than conventional hydrocracking and requires temperatures slightly higher than hydrotreating. This process is economically very attractive, since it allows for increasing the production of middle distillates by using existing hydrotreaters and therefore is without expensive investment costs (2). Catalysts used in MHC contain the combination of two nonnoble metals, such as Ni (or Co) and Mo (or W), supported on an acidic carrier, such as amorphous silica–alumina, halogen-doped alumina, or zeolites (3). Hence, the catalysts are similar to those used for hydrotreating but with acidic properties that are needed to crack the heavy hydrocarbons. Zeolite-based hydrocracking catalysts are more active and less sensitive to deactivation by coking and basic nitrogen compounds than amorphous-based catalysts (4), although the former are less selective to middle distillates owing to the presence of stronger acid sites, which favors the recracking to produce naphtha and gases (5). Therefore, and from the point of view of maximizing middle distillates, it would be highly desirable to design hydrocracking catalysts that combine the good activity of the zeolite-based catalysts with the selectivity of the amorphous silica–alumina.

On the other hand, increasing the cetane number of low-quality diesel fractions involves a severe reduction of their aromatic content (6). If a deep aromatic saturation has to be performed, highly active hydrogenation catalysts working at moderate temperatures have to be prepared. Noble metals are good hydrogenation catalysts, but unfortunately they

[1] To whom correspondence should be addressed. Fax: (+34) 96 3877809. E-mail: acorma@itq.upv.es.

0021-9517/01 $35.00

are easily poisoned with small amounts of sulfur present in the feed. Therefore, these catalysts are typically used in the second reactor of a two-stage process, in which a severe reduction of the sulfur content—up to a few parts per million—takes place in the first reactor (6, 7). The sulfur tolerance is, consequently, an important factor in this type of catalyst, since it determines the catalyst's life and/or the severity to be used in the first stage of the process. In this sense, it has been reported that the sulfur resistance of Pt(Pd)-based catalysts is significantly improved when supported on an acidic zeolite (6–8). Thus, Pt(Pd)-zeolite catalysts show relatively high hydrogenation activity even in the presence of several hundred parts per million sulfur. However, the presence of an essentially microporous system in zeolites hinders the diffusion of polyaromatic molecules present in commercial feeds to the active sites, limiting the activity of zeolite-based hydrogenation catalysts.

In this sense, the use of materials that combine characteristics of zeolites, such as an ordered structure and a high surface area, along with other properties usually related to amorphous materials, such as large pores that allow the diffusion of bulky molecules, could represent a clear benefit in certain refining processes dealing with heavy feedstocks. Following this reasoning, we have shown that catalysts based on the new mesoporous MCM-41 material display excellent activity and selectivity in both mild hydrocracking (9) and aromatic hydrogenation reactions (10). Up to now, the most successful solutions to increase the diffusivity in zeolites relied on the modification of their textural properties by postsynthesis treatments (e.g., calcination in the presence of steam) or by reducing the average size of the crystallites by direct synthesis (11, 12). In this line of work, we have recently reported that a nanocrystalline β zeolite-based catalyst displayed high activity and good selectivity toward middle distillates during the mild hydrocracking of vacuum gasoil (13).

Very recently our group prepared a new material (14), obtained by delaminating the layered zeolite precursor of the MWW structure and denoted as ITQ-2, which consists of thin sheets 2.5 nm in height. The sheets present a hexagonal array of "cups" (0.7×0.7 nm) that penetrate into the sheet from both sides and a double 6 MR windows connects the bottoms of the cups located in the opposite side of the sheet. The structure of this material also presents a circular 10 MR channel system inside the sheet. Owing to its peculiar structure, ITQ-2 shows an extremely high and well-defined external surface area (>700 m^2/g), which facilitates the access of voluminous molecules during the cracking of vacuum gasoil (15).

In this work we have studied the catalytic performance of ITQ-2-based catalysts for the mild hydrocracking of vacuum gasoil (NiMo/ITQ-2) and the hydrogenation of aromatics (Pt/ITQ-2). The results are compared with those obtained with other conventional supports, e.g., amorphous silica–alumina (ASA), γ-Al_2O_3, and ultrastable Y zeolite (USY).

2. EXPERIMENTAL

2.1. Catalysts

An ITQ-2 material (Si/Al = 50) was prepared following the procedure described in Ref. (16). The layered MWW precursor was prepared using hexamethylenimine (HMI) (Aldrich, 99%), silica (Aerosil 200, Degussa), sodium aluminate (56% Al_2O_3, 37% Na_2O, Carlo Erba), sodium hydroxide (98% Prolabo), and deionized water. The gel of composition $0.5\,HMI : 44.9\,H_2O : 0.18\,Na : 0.16\,OH : 0.010\,Al_2O_3 : SiO_2$ was crystallized at 135°C for 11 days. Then, the solid was separated by centrifugation, washed with deionized water, and dried at 60°C overnight. This material (layered precursor) was swelled with hexadecyltrimethylammonium bromide ($HTMA^+$). After the completion of swelling, an increase in the distance between the layers from 2.7 nm to approximately 4.5 nm was observed by X-ray diffraction. The layers are forced apart by placing the slurry in an ultrasound bath (50 W, 40 kHz) for 1 h. Subsequently, addition of a few drops of concentrated hydrochloric acid allowed gathering of the solids by centrifugation. After elimination of the organic material by calcination at 540°C, the ITQ-2 material was finally obtained.

For comparison purposes, the following materials were also used as supports: an amorphous silica–alumina (ASA) sample (Crossfield, 25 wt% Al_2O_3); a USY zeolite (CBV760, PQ Corp., $a_0 = 2.426$ nm, bulk Si/Al = 28); and γ-Al_2O_3 (Merk).

NiMo-containing catalysts were prepared by impregnation using the sequential pore filling method with the required amount of ammonium heptamolybdate (AHM) and nickel nitrate (NN) aqueous solutions so as to obtain catalysts with 12 wt% MoO_3 and 3 wt% NiO. After impregnation with AHM, the samples were calcined at 500°C for 3 h, then impregnated with NN, and calcined again as above.

Pt-supported catalysts were prepared by impregnation of supports with an excess (3 mL solution/g solid) of a 0.2 M HCl aqueous solution of hexachloroplatinic acid, followed by evaporation of the solvent in a rotary evaporator, drying at 100°C, calcination at 500°C for 3 h, and finally reduction in H_2 at 450°C for 1 h before starting the catalytic experiments. Samples prepared and activated by this method are denoted as Pt(A)/S(H), where S is the support (S = ITQ-2, USY, ASA, and γ-Al_2O_3). In the case of ITQ-2 and USY, samples were also prepared by the same impregnation method but activated at lower temperatures, i.e., 350°C calcination and 350°C reduction. Those samples were denoted as Pt(A)/S(L). In this way, samples containing 0.5 wt% Pt (for naphthalene and benzene hydrogenation)

and 1 wt% Pt (for LCO hydrogenation) were prepared. In the case of USY support, a catalyst was also prepared using the incipient wetness impregnation technique (pore filling), followed by drying, calcination at 500°C, and reduction at 450°C. This sample was denoted as Pt(B)/USY(H).

2.2. Characterization of Catalysts

X-Ray diffraction measurements were performed with Phillips X'PERT equipment with automatic slits using Cu$K\alpha$ radiation. Nitrogen adsorption isotherms at −196°C were obtained in an ASAP 2000 apparatus after pretreating the samples under vacuum at 400°C overnight. The acidity of the samples was measured by IR spectroscopy with adsorption of pyridine and desorption at different temperatures in a Nicolet 710 FTIR equipment following the experimental procedure described in Ref. (17). The concentrations of Lewis and Brønsted acid sites were estimated from the intensity of the IR bands at ca. 1545 and 1450 cm^{-1}, respectively, using the integrated molar extinction coefficients given by Emeis (18). Hydrogen chemisorption experiments were performed at 20°C using the pulse flow method in a Chemisorb 2700 apparatus after reducing the catalysts in hydrogen at 450°C (for samples calcined at 500°C) or at 350°C (for samples calcined at 350°C) for 2 h.

2.3. Reaction Systems and Procedures

Mild hydrocracking of vacuum gasoil (VGO) was carried out in a fixed-bed stainless-steel tubular reactor having a 2.54-cm i.d and 65-cm length. The reactor was charged with 5 g of catalyst with a particle size of 0.59- to 0.84-mm diameter previously diluted with SiC (diluent/catalyst weight ratio of 6). The catalysts were presulfided using a mixture of H_2S/H_2 (10 vol% H_2S) at atmospheric pressure and 400°C for 3 h. The reaction conditions were the following: 3.0 MPa total pressure, 350–450°C reaction temperature, WHSV = 2 h^{-1}, and H_2/feed ratio = 1000 Nm^3/m^3. In each run, liquid samples were accumulated, weighed, and analyzed at intervals of about 1 h. For all catalysts, a constant composition of products was observed after reaction periods of 6–10 h. The results reported in this work correspond to the steady-state period of operation. The distillation curves in the original feed and liquid reaction products were determined by simulated distillation (SIMDIS, ASTM D-2887) in a Varian GC 3400. The main physicochemical characteristics of the VGO feed are given in Table 1.

Hydrogenation of naphthalene as a model compound was carried out in a 0.5-L batch reactor (Autoclave Engineers, Inc.) equipped with a reactant loader for a good zero-time determination, and with inlet and outlet valves for adding and removing gases and liquid samples. In all cases, 1 g of catalyst of 0.10- to 0.25-mm particle diameter was reduced *ex situ* at 350 or 450°C for 1 h in a H_2 flow (250 mL/min) and immediately transferred to the batch reactor and heated in hydrogen atmosphere up to the desired reaction temperature. Then, 100 g of a solution of 10 wt% of naphthalene (Meck, >98%) in *n*-decane (Arcross, >99.5%) was added to the reactor and the system was pressurized with H_2 up to the desired reaction pressure. The reaction conditions in these experiments were the following: 275°C reaction temperature, 5.0 MPa total pressure, and stirring speed of 1000 rpm. Liquid samples were taken at different reaction times and analyzed on a gas chromatograph (Varian 3400) equipped with a flame ionization detector (FID) and a capillary column (Supelco SPB-1, 30 m length). The sulfur tolerance of the Pt catalyst was studied by adding to the reactant solution 200 ppm of sulfur as dibenzothiophene.

Additional benzene hydrogenation experiments were carried out to study the location/accessibility of Pt in Pt/USY and Pt/ITQ-2 catalysts. The experiments were performed in a fixed-bed microreactor at 150°C, 4.0 MPa total pressure, H_2/benzene molar ratio of 8, and space velocity (WHSV) in the range 8–32 h^{-1}. Under the reaction conditions used, cyclohexane was the only product observed in the benzene hydrogenation experiments.

In a second part, the hydrogenation of a previously hydrotreated light cycle oil (HT-LCO) was carried out in the same fixed-bed reactor described above for the mild hydrocracking experiments. Hydrotreatment of the original LCO was performed, to reduce the sulfur content, using a commercial hydrotreating catalyst (TK-525, Haldor-Topsoe) at 400°C, 3.0 MPa, WHSV = 0.3 h^{-1}, and H_2/feed ratio = 1000 Nm^3/m^3. The main characteristics of the original LCO and the hydrotreated feed (HT-LCO) are included in Table 1. The reactor was charged with 2.5 g of Pt-catalyst, having a particle size of 0.59–0.84 mm previously diluted with SiC (inert/catalyst weight ratio of 6). Before starting each run the catalyst was reduced at 400°C for 2 h in hydrogen flow of 0.5 L/min at atmospheric pressure. The reaction conditions for the hydrogenation of the HT-LCO were: 300 and 350°C reaction temperature, 5.0 MPa total pressure, WHSV = 4h^{-1}, and hydrogen/feed ratio = 1000 Nm^3/m^3. The catalytic data reported correspond to reaction times above 6 h on stream, for which stationary state was achieved. The content and distribution of aromatics in the feed and products were determined by gas chromatography in a Varian GC3400 equipped with a FID, a capillary column (Petrocol DH-100, 100-m length), and a mass spectrometer to identify the aromatic components.

In all cases preliminary tests were carried out to ensure that under the reaction conditions used the reaction rate was controlled neither by external nor by intraparticle mass transfer limitations.

The concentrations of sulfur and nitrogen in the original feed and liquid products were determined by elemental analysis in a Fisons 1108 CHNS-O instrument.

TABLE 1

Properties of Vacuum Gasoil (VGO), Light Cycle Oil (LCO), and Hydrotreated LCO (HT-LCO)

	Feedstock		
	VGO	LCO	HT-LCO
Nitrogen (ppm)	2900	643	480
Sulfur (wt%)	2.53	1.60	0.40
Density (g cm^{-3}) (15°C)	0.917	0.917	—
Distillation curve			
IBP	211	64	58
5%	330	173	147
10%	356	206	177
20%	382	229	208
30%	399	244	228
40%	411	258	241
50%	422	271	254
60%	432	289	272
70%	444	306	289
80%	458	328	307
90%	475	349	337
95%	486	370	361
FBP	509	467	451

3. RESULTS AND DISCUSSION

3.1. Characterization of Catalysts

The X-ray diffraction pattern of the ITQ-2 sample (not shown) does not show the 001 and 002 peaks at $2\theta = 3°–7°$ of the characteristic 2.5-nm periodicity typical of the MWW topology, in agreement with the proposed structure (14), as shown in Fig. 1. Moreover, ITQ-2 presents broader high-angle peaks than the MWW precursor, which is coherent with a reduction of the long-range order on exfoliation of the MCM-22 precursor (14).

The textural and acidic properties of the different supports are summarized in Table 2. It is worth noting the high total surface area ($\approx$900m^2 g^{-1}) and the large proportion of mesopores in the ITQ-2 material, in agreement with the proposed structure of sheets randomly arranged and mainly edge-to-face (Fig. 1). As previously reported (14) ITQ-2 is formed by single layers organized in a "house of cards"-type structure, which defines a material with a high and well-structured external surface area. As observed in Table 2, ITQ-2 shows a substantially higher surface area and pore volume than the rest of the supports, especially if we

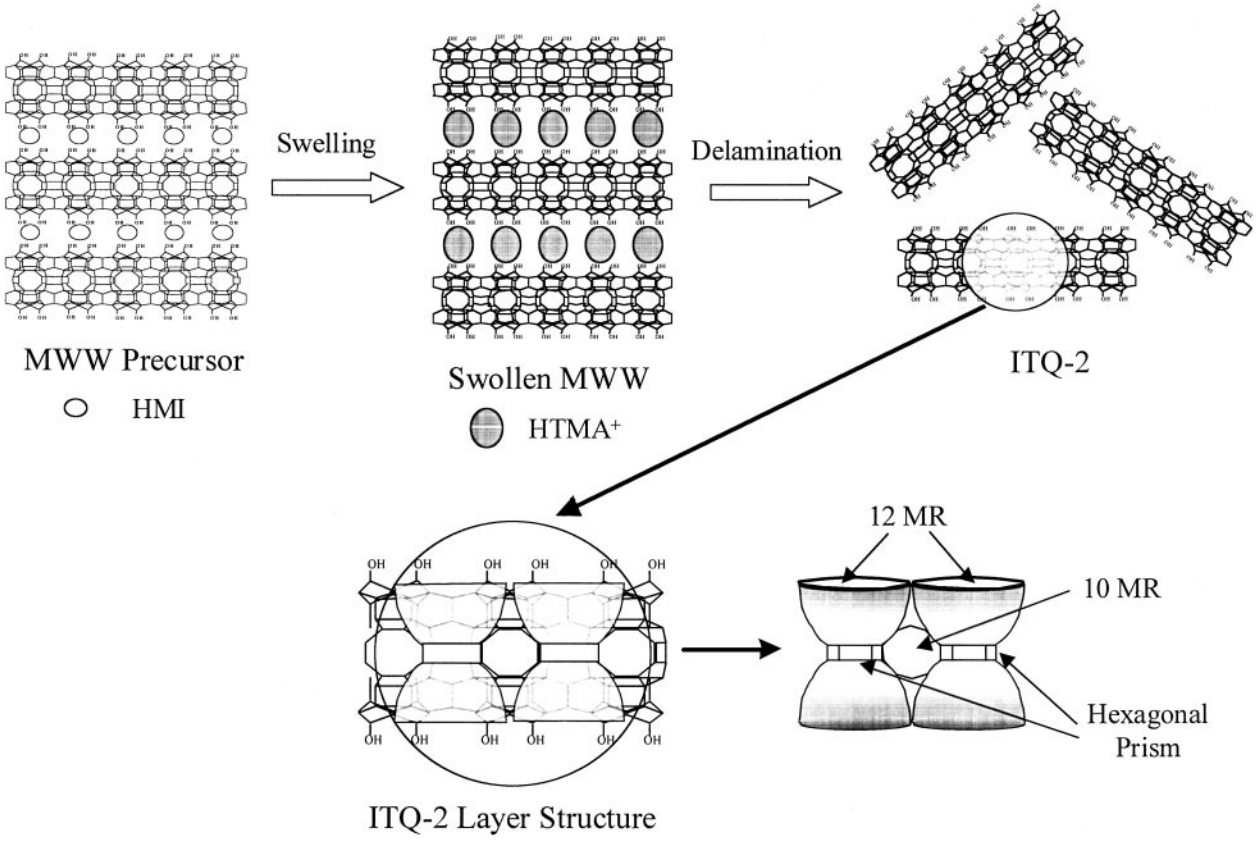

FIG. 1. Scheme of the preparation and proposed structure of ITQ-2, showing an artist's impression of the arrays of cups.

TABLE 2

Textural Properties and Acidity of the Different Supports

	Textural properties[a]				Acidity (μmol pyridine g^{-1})[b]			
	BET surface area ($m^2\ g^{-1}$)		Pore volume ($cm^3\ g^{-1}$)		Brønsted		Lewis	
Support	Total	Micropore	Total	Micropore	250°C[c]	350°C[c]	250°C[c]	350°C[c]
ITQ-2	895	60	0.99	0.04	17.0	6.8	24.1	15.5
USY	551	362	0.41	0.18	20.4	8.3	11.7	7.6
ASA	268	21	0.31	<0.01	5.3	1.1	22.2	12.8
γ-Al_2O_3	122	2	0.21	<0.01	—	—	—	—

[a] Determined by nitrogen adsorption–desorption experiments.
[b] Measured by IR spectroscopy with adsorption of pyridine and desorption at different temperatures. Values of μmol pyridine g_{cat}^{-1} calculated using the extinction molar coefficients given by Emeis (18).
[c] Desorption temperature.

compare with the amorphous silica–alumina (ASA) and γ-Al_2O_3 materials having most of their pores in the meso- and macropore range. By contrast, the USY zeolite presents the highest microporosity, although some mesoporosity, probably originated during the hydrothermal treatments, is also observed (Table 2).

The acidity of the supports is also presented in Table 2. It is seen that the delaminated ITQ-2 material shows some lower Brønsted acidity than USY zeolite, with most of the sites being of medium-strong acidity. The similarity in acid strength distribution can be explained by taking into account the zeolitic nature of ITQ-2, although a decrease in Brønsted acidity during the delamination process has been observed (14). On the other hand, the ASA shows a significantly lower Brønsted acidity, with most of the sites being of weak-medium strength.

The acidic and textural properties of the NiMo-supported catalysts are shown in Table 3. In all cases there is a significant reduction of surface area after the incorporation of the metals, the decrease being especially pronounced for the ITQ-2 and USY samples. The loss of surface area might be related to a partial destruction of zeolitic structure and/or pore blockage produced mainly after the impregnation of Mo (19, 20). Moreover, a decrease in the Brønsted acidity is observed after the impregnation of the NiMo phases (Table 3). This has been ascribed to the interaction of the metal precursors with surface OH groups of the supports during the impregnation step (21), although partial destruction of the crystalline structure in ITQ-2 and USY zeolites could also contribute to the decrease in Brønsted acidity in these catalysts.

By contrast, when those materials have been used to prepare the hydrogenation catalysts, we have seen that their textural and acidic properties hardly changed after the impregnation of Pt (not shown). The metal dispersion of the Pt-supported catalysts has been measured from the H_2 uptake capacity, assuming that the irreversible adsorption of hydrogen takes place dissociatively with a stoichiometry of $H_2/Pt = 1/2$, and thus the H_{irr}/Pt ratio represents the fraction of exposed surface Pt atoms. The H_{irr}/Pt ratios obtained for the different Pt-containing catalysts (0.5 wt% Pt) prepared are given in Table 4. For samples prepared by wet impregnation and calcined at 500°C and reduced at 450°C the metal dispersion decreases in

TABLE 3

Textural Properties and Acidity of the Different NiMo-Supported Catalysts

	Textural properties[a]				(Acidity μmol pyridine g^{-1})[b]			
	BET surface area ($m^2\ g^{-1}$)		Pore volume ($cm^3\ g^{-1}$)		Brønsted		Lewis	
Catalyst	Total	Micropore	Total	Micropore	250°C[c]	350°C[c]	250°C[c]	350°C[c]
NiMo/ITQ-2	472	43	0.68	0.02	5.1	1.7	19.8	6.8
NiMo/USY	427	348	0.29	0.09	8.4	5.6	22.7	9.3
NiMo/ASA	171	15	0.29	<0.01	0.5	<0.1	3.5	0.3
NiMo/γ-Al_2O_3	104	<1	0.16	<0.01	—	—	—	—

[a] Determined by nitrogen adsorption–desorption experiments.
[b] Measured by IR spectroscopy with adsorption of pyridine and desorption at different temperatures. Values of μmol pyridine g_{cat}^{-1} calculated using the extinction molar coefficients given by Emeis (18).
[c] Desorption temperature.

TABLE 4

Results of H_2 Chemisorption Experiments for Pt-Supported Catalysts Prepared and Activated under Different Conditions

Sample	Method of Pt impregnation[a]	Temperature (°C) Of calcination	Of reduction	ratio H_{irr}/Pt
Pt(A)/ITQ-2(H)	A	500	450	0.80
Pt(A)/ASA(H)	A	500	450	0.20
Pt(A)/γ-Al_2O_3(H)	A	500	450	0.75
Pt(A)/USY(H)	A	500	450	0.15
Pt(B)/USY(H)	B	500	450	0.66
Pt(A)/USY(L)	A	350	350	0.75
Pt(A)/ITQ-2(L)	A	350	350	0.84

[a] A = wet impregnation, B = incipient wetness impregnation.

the following order (H_{irr}/Pt ratios in parentheses): Pt/ITQ-2 (0.80) > Pt/Al_2O_3 (0.75) > Pt/ASA (0.20) > Pt/USY (0.15). The high H_{irr}/Pt ratio obtained for the Pt/ITQ-2 sample indicates a high degree of metal dispersion, which can be ascribed to its high surface area and mesoporosity. A high Pt dispersion is also observed for the Pt/γ-Al_2O_3 catalyst. Usually, this has been explained considering that the Pt clusters are strongly held on the platelets of γ-Al_2O_3 (22), thus favoring the metal dispersion and avoiding sintering of the metal particles during the activation treatments. Both Pt/USY and Pt/ASA catalysts show much lower Pt dispersions. A better Pt dispersion in USY (H_{irr}/Pt = 0.66) was obtained when the metal was impregnated using the incipient wetness technique (sample Pt(B)/USY(H)). Besides the method of impregnation, the calcination and reduction temperatures are also important parameters affecting metal dispersion in Pt/zeolite catalysts (23). Thus, when Pt/USY prepared by wet impregnation was calcined at 350°C and reduced at 350°C (sample Pt(A)/USY(L)) the dispersion significantly increased (H_{irr}/Pt = 0.75), as observed in Table 4. In the case of Pt/ITQ-2, the lower calcination and reduction temperature also increased the already high Pt dispersion.

3.2. Catalytic Experiments

3.2.1. Mild hydrocracking of vacuum gasoil on NiMo-containing catalysts. In this part of the work we studied the performance of the NiMo/ITQ-2 catalyst for the mild hydrocracking (MHC) of VGO, and compared the results with those obtained for NiMo/ASA, NiMo/USY, and NiMo/γ-Al_2O_3 catalysts under the same reaction conditions and having the same metal loadings (see Experimental). An important goal in MHC is, besides maximizing middle distillates, to achieve as much reduction in heteroatoms (mainly sulfur and nitrogen) as possible. Figure 2 shows the hydrodesulfurization (HDS), hydrodenitrogenation (HDN), and hydrocracking (HC) conversions as a function of reaction temperature for the different NiMo-containing catalysts. The hydrocracking conversion was calculated considering as products the fraction of compounds with boiling points below 360°C and the fraction boiling above this temperature as unreacted feed.

As observed, the NiMo/γ-Al_2O_3 catalyst is, by far, the most active catalyst for HDN and HDS reactions (Figs. 2c and 2b, respectively) in the entire range of

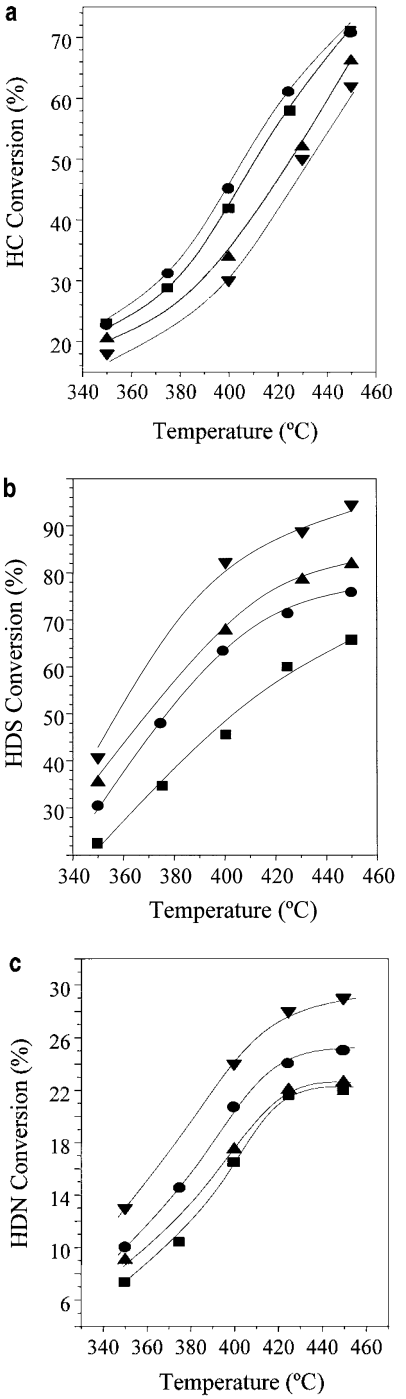

FIG. 2. (a) Hydrocracking (HC), (b) hydrodesulfurization (HDS), and (c) hydrodenitrogenation (HDN) conversions obtained for the different catalysts as a function of reaction temperature. Reaction conditions: 3.0 MPa, 2 h^{-1} WHSV, and 1000 H_2 (STP)/feed ratio. (●) NiMo/ITQ-2, (■) NiMo/USY, (▲) NiMo/ASA, (▼) NiMo/γ-Al_2O_3.

temperatures studied. This is not surprising taking into account that alumina-based catalysts are currently used in most commercial hydrotreatment processes. The efficient heteroatom removal of the alumina-based catalyst has been frequently ascribed to a good dispersion of the metals and to appropriate metal–support interaction (24, 25), which may favor the formation of the active NiMoS phase on sulfidation (26). In fact, the catalyst based on ASA (containing 25 wt% Al_2O_3) gives a higher HDS activity than the catalysts based on silicon-rich supports, such as ITQ-2 and USY zeolites. Nevertheless, NiMo/ITQ-2 is more active for HDS than NiMo/USY. On the other hand, NiMo/ITQ-2 also gives a higher HDN activity than NiMo/ASA and NiMo/USY (Fig. 2c). Some authors have reported an enhanced activity for removal of N considering a synergetic cooperation between Brønsted acid sites in the support and the sulfide phases (27), although this cannot account for the higher HDN activity of ITQ-2 as compared with USY-based catalysts, both supports having similar acidity (Table 2). The relatively high HDS and HDN activities of the ITQ-2-based catalyst could be explained by taking into account the higher external surface area and mesoporosity of the delaminated ITQ-2 material, thus favoring the metal dispersion and the accessibility of reactants to the metal active phases.

With respect to hydrocracking activity, both NiMo/ITQ-2 and NiMo/USY are the most active catalysts, with the former being slightly more active in the range 375–425°C (Fig. 2a). This is not surprising taking into account the higher Brønsted acidity of the zeolite-based catalysts as compared with the amorphous ones (Table 3). In this respect, the relatively high hydrocracking activity observed for the γ-Al_2O_3-based catalyst, which according to some authors may be ascribed to the formation of –SH groups presenting Brønsted acidity in the metal sulfide phase (28), has to be noted. Nevertheless, Brønsted acidity by itself cannot account for the higher activity of NiMo/ITQ-2 as compared with the more acidic NiMo/USY. Again, the peculiar structure of ITQ-2 presenting a large external surface area and mesoporosity, in contrast to the higher microporosity of the USY zeolite, might explain the above catalytic results.

The product selectivity of the ITQ-2-, USY-, and ASA-based catalysts at 50–55% HC conversion is compared in Table 5. Note here that the hydrocracking conversion in these experiments was varied by changing the reaction temperature. Thus, the temperature needed to obtain 50–55% conversion increased from ca. 410°C for the most active NiMo/ITQ-2 catalyst to ca. 440°C for the less active NiMo/γ-Al_2O_3. NiMo/ITQ-2 shows a low selectivity to gases, similar to that of the amorphous NiMo/ASA sample and significantly lower than that of NiMo/USY. With respect to liquid products, the selectivity to naphtha of NiMo/ITQ-2 is similar to that of NiMo/USY, while the selectivity to middle distillates of the ITQ-2-based catalyst is intermediate between those of NiMo/ASA and NiMo/USY.

TABLE 5

Selectivity of the Different Hydrocracked Fractions Obtained at ca. 55% Hydrocracking Conversion over NiMo-Containing Catalysts[a]

Catalyst	Gases	Naphtha	Middle distillates
NiMo/ITQ-2	14.1	34.3	51.6
NiMo/USY	18.9	34.1	47.0
NiMo/ASA	14.5	32.4	53.1

[a] Gases: C_1–C_4; naphtha: C_4, 195°C; middle distillates: 195–360°C.

The higher selectivity to gases of NiMo/USY can be attributed to a higher recracking produced inside the micropores of the zeolite owing to the higher Brønsted acidity (Table 3), and to the lower diffusion rate of products inside the microporous system. This fact does not affect the ITQ-2 material, where reactants and products can easily diffuse from the sheet to the exterior or vice versa, resulting in reduced recracking probability.

These results clearly illustrate the advantages of using the delaminated ITQ-2 material as support for preparing NiMo-based hydrocracking catalysts. The particular structure of ITQ-2 allows for combining the high activity typical of zeolite-based catalysts with the good selectivity of amorphous catalysts.

3.2.2. Hydrogenation of naphthalene on Pt-supported catalysts. The hydrogenation of naphthalene produces mainly tetralin, *cis*-decalin, and *trans*-decalin according to the proposed reaction network (Fig. 3). Under our reaction conditions (275°C, 5.0 MPa), the formation of hydrogenated products can be considered as irreversible reaction (29). The change in concentrations of the naphthalene reactant and reaction products with reaction time is shown in Fig. 4a for the Pt/ITQ-2 catalyst. As seen there, the main product obtained in the hydrogenation of naphthalene under the given conditions is tetralin, with decalins being formed in significant amounts only at longer reaction times. This tendency is more clearly reflected in Fig. 4b, where the selectivity to tetralin and decalins is plotted as a function of naphthalene conversion. The selectivity to

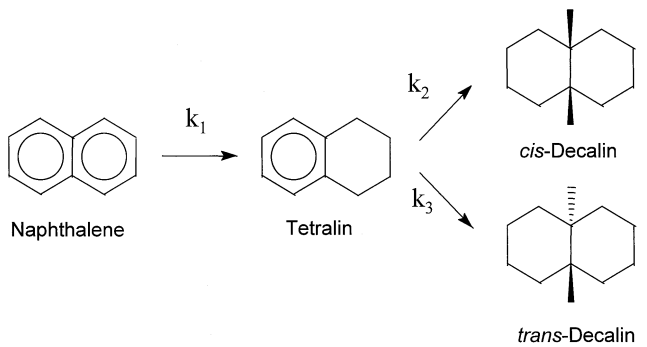

FIG. 3. General reaction network for naphthalene hydrogenation.

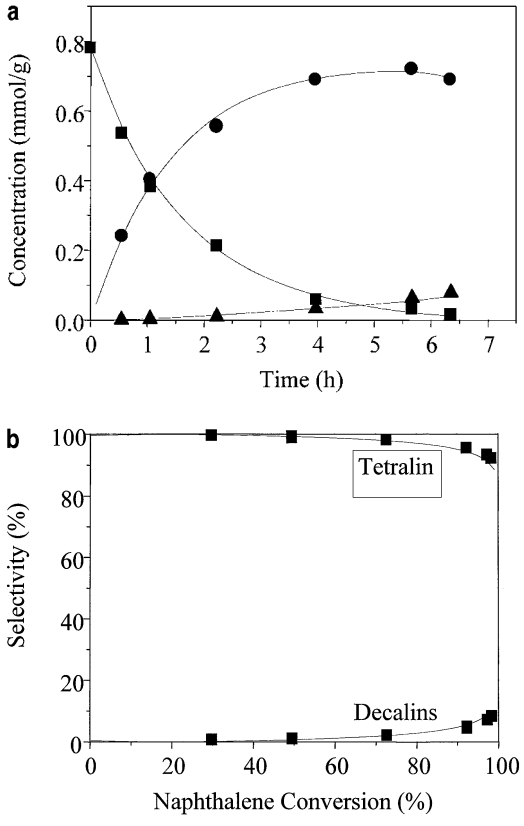

FIG. 4. Hydrogenation of naphthalene over Pt/ITQ-2 at 275°C and 5.0 MPa. (a) Concentration of reactant (■) and products (● tetralin, ▲ decalins) as a function of reaction time. (b) Selectivity to tetralin and decalins as a function of naphthalene conversion.

decalins is appreciable only for very high naphthalene conversions (>80%), which clearly indicates the secondary character of these products.

Under the reactions conditions studied here, irreversible reactions and large excess of hydrogen, and by assuming that the hydrogenation of aromatic compounds follows a pseudo-first-order dependence on hydrocarbon reactant, the following kinetic equation can be obtained:

$$-\ln(1 - X_{\text{naphthalene}}) = k_1 t.$$

The corresponding data obtained for Pt/ITQ-2 are plotted in Fig. 5. As observed, the experimental data fit very well the above kinetic expression, allowing calculation of the pseudo-first-order kinetic rate constants for hydrogenation of naphthalene. Similar correlations were obtained for the rest of the catalysts. The kinetic constant values for the hydrogenation of the first ring (k_1) of naphthalene at 275°C are compared in Table 6 for the different Pt-supported catalysts. For catalysts calcined at 500°C and reduced at 450°C Pt/ITQ-2, presenting the largest Pt dispersion, shows the highest activity for hydrogenation of naphthalene. The

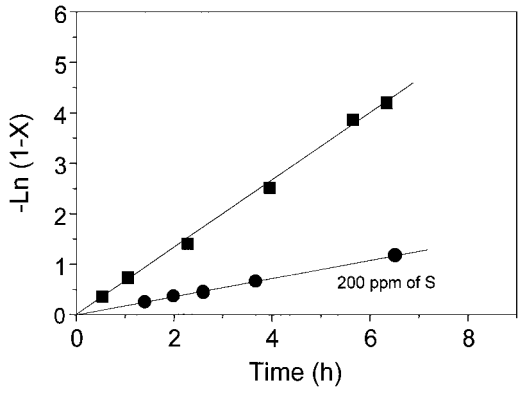

FIG. 5. Pseudo-first-order kinetic fit for naphthalene hydrogenation over Pt/ITQ-2 in the absence and the presence of 200 ppm sulfur. Reaction conditions as in Fig. 6.

relatively low hydrogenation activity of Pt/USY is ascribed to its poor metal dispersion, as discussed before. Nevertheless, Pt/ITQ-2 is more active than Pt/γ-Al_2O_3 despite the fact that both catalysts present similar Pt dispersions. Therefore, other factors such as the presence of a well-defined micro-/mesoporous structure and especially different adsorption properties in the delaminated zeolite might contribute to the enhanced hydrogenation activity of Pt/ITQ-2 with respect to Pt/γ-Al_2O_3. As expected, the hydrogenation activity of Pt/USY catalysts is significantly increased when improving the metal dispersion either by changing the method of impregnation (sample Pt(B)/USY(H)) or by calcining and reducing at lower temperatures (sample Pt(A)/USY(L)). Also in the case of Pt/ITQ-2 the hydrogenation activity increases when the impregnated sample is calcined and reduced at lower temperatures (350°C). In any case, it appears that for samples activated at lower temperatures and presenting highly dispersed Pt particles, Pt/USY is more active for hydrogenation of naphthalene than Pt/ITQ-2.

Moreover, when the turnover frequency (TOF), that is, the activity per exposed surface metal atom, is compared

TABLE 6

Kinetic Rate Constant for the Hydrogenation of the First Ring of Naphthalene (k_1) and Turnover Frequency (TOF) on the Different Pt-Supported Catalysts[a]

Catalyst	$k_1 \times 10^4$ ($s^{-1}\,g_{cat}^{-1}$)	TOF
Pt(A)/ITQ-2(H)	1.82	9
Pt(A)/γ-Al_2O_3(H)	1.63	8
Pt(A)/ASA(H)	1.47	29
Pt(A)/USY(H)	1.54	40
Pt(A)/USY(L)	4.51	24
Pt(B)/UYS(H)	3.05	18
Pt(A)/ITQ-2(L)	3.64	17

[a] Reaction conditions: 275°C, 5.0 M.

for the different catalysts (Table 6), Pt/USY clearly shows the highest intrinsic activity irrespective of the preparation and activation conditions while the catalysts based on ITQ-2 and γ-Al_2O_3 give the lowest TOF values. The higher turnover displayed by Pt/USY could be explained by taking into account the formation of a bidisperse metallic phase, with large aggregates being formed on the external zeolite surface and small Pt clusters (about 1 nm size) fitting the supercages of the Y zeolite (30). These small clusters interacting closely with the zeolite framework may contain electron-deficient Pt species formed by electron transfer from Pt to the zeolite acid sites, which would enhance catalytic activity toward hydrogenation reactions (31–36). Moreover, an additional contribution to the overall hydrogenation rate by hydrogen spilled over from the metal to the aromatic ring adsorbed on the acid site of the support could also explain the high specific activity of the USY-based catalyst (31–34).

Nevertheless, the acidity of the support must not be the unique parameter to be considered to explain the hydrogenation activity of the Pt-supported catalysts. Indeed, Pt/ASA shows a relatively high TOF (Table 6) and its acidity is relatively low (Table 2), while both Pt/ITQ-2 and Pt/USY show similar acidity but the former presents a lower specific activity. Therefore, other parameters such as the location and shape of metal particles and the pore geometry of the support also contribute to the final activity, as will be shown later.

The kinetic rate constants for the hydrogenation of the second ring (k_2, k_3) were obtained assuming that the hydrogenation of tetralin into decalins follows a pseudo-first-order dependence. For all catalysts studied the $k_1/(k_2 + k_3)$ ratio was ca. 30 under our reaction conditions. As expected, the hydrogenation rate for the second ring of naphthalene is much slower than the hydrogenation of the first ring, in good agreement with the values reported in the literature (37). On the other hand, it has to be pointed out that the *cis*-/*trans*-decalin ratios (values not shown) were always higher than those predicted by the thermodynamic equilibrium, suggesting that the formation of *cis*-decalin is kinetically favored (38).

To compare the sulfur resistance of Pt/ITQ-2 with that of the rest of the catalysts studied 200 ppm of sulfur was added as dibenzothiophene to the *n*-decane/naphthalene feed mixture. The kinetic results obtained for the Pt/ITQ-2 catalyst are shown in Fig 5. As observed, the data obtained in the presence of sulfur could also be fitted to a pseudo-first-order kinetic expression, and this was so for the rest of catalysts studied. The kinetic rate constants in the presence of sulfur (k_1') were thus obtained as explained before for the sulfur-free experiments. The sulfur resistance obtained for the series of catalysts calcined at 500°C and reduced at 450°C, measured as the ratio between the hydrogenation constants for the first ring of naphthalene in the presence and in the absence of sulfur (k_1'/k_1 in parentheses), decreased in the order Pt/USY (0.60) > Pt/ITQ-2 (0.32) > Pt/γ-Al_2O_3 (0.17) > Pt/ASA (0.13). As could be expected, the zeolite-based catalysts (USY, ITQ-2) are more sulfur resistant than the amorphous ones (ASA, alumina) (39). This fact has been currently attributed to the interaction between the zeolite Brønsted acid centers and the metal sites producing electron-deficient metal particles that are more resistant to poisoning by sulfur (40, 41). Nevertheless, Pt/USY is significantly more thioresistant than Pt/ITQ-2, despite their similar acidity. As suggested before, the small Pt clusters located in the supercavities of the Y zeolite should present a stronger metal–support interaction than in the case of the larger metal crystallites formed on the surface of ITQ-2.

3.2.2. Hydrogenation of benzene. It has been shown above that for samples having the same total Pt content and comparable Pt dispersions Pt/USY is more active than Pt/ITQ-2 for the hydrogenation of naphthalene. This could be explained considering that some of the Pt atoms in Pt/ITQ-2 are located in the independent 10 MR channel system and that these are hardly accessible for the naphthalene reactant molecules, which can easily diffuse through the larger pores of USY. To test the above hypothesis we also carried out the hydrogenation of a smaller aromatic molecule, i.e., benzene, which, contrarily to naphthalene, can diffuse through the 10 MR channels of ITQ-2 and reach the Pt sites located there. The pseudo-first-order kinetic curves obtained for the hydrogenation of benzene on Pt(A)/USY(L) and Pt(A)/ITQ-2(L) catalysts calcined and reduced at 350°C (having comparable Pt dispersions) are plotted in Fig. 6. From the slopes of the fitted curves it was found Pt/ITQ-2 is ca 3.8 times more active than Pt/USY for benzene hydrogenation, while for naphthalene hydrogenation the latter is 1.25 times more active.

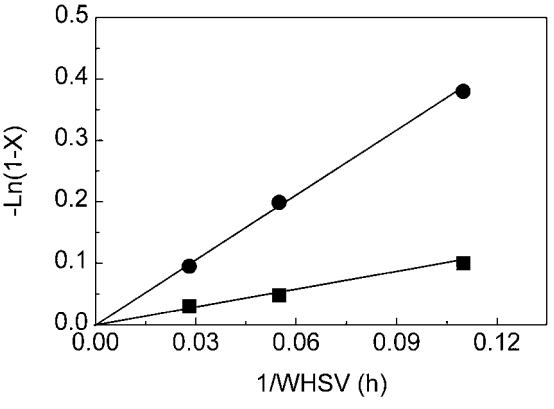

FIG. 6. Pseudo-first order kinetic fit for benzene hydrogenation over Pt/USY (■) and Pt/ITQ-2 (●) catalysts calcined and reduced at 350°C. Reaction conditions: 150°C, 4.0 MPa total pressure, H_2/benzene = 8 mol/mol, and 1/WHSV in the range 0.03–0.11 h.

3.2.3. Hydrogenation of light cycle oil. In the last part of the work we studied the hydrogenation of a LCO over Pt (1 wt%) supported on delaminated ITQ-2, USY, and ASA. LCO, which is produced in FCC units, is a diesel range fraction with high aromatic content (∼70 vol%) and significant amounts of sulfur (1–2 wt%) and nitrogen (1000–400 ppm) compounds. Before using LCO as a diesel-blending component, it is necessary to upgrade this fraction by reducing both aromatics and sulfur. Owing to its high sulfur content, a dual-stage hydrogenation process has to be used where the feed is first hydrotreated to reduce its sulfur content, and then hydrogenated using a noble metal catalyst in the second reactor. To simulate the dual-stage process we first carried out the hydrotreatment of the LCO feed using a commercial CoMo/alumina catalyst (TK550, Haldor-Topsoe) under the conditions described under Experimental. The sulfur content was thus reduced from 1600 ppm in the LCO feed to 400 ppm in the hydrotreated product (Table 1). On the other hand, the total aromatic content remained at similar levels, with a slight decrease from 71 to 68%, while the fraction of monoaromatics increased from 21 to 24 wt%. Besides this, partial hydrocracking of the LCO also occurred during the hydrotreatment. The total aromatic content and the aromatic distribution obtained during the hydrogenation of the HT-LCO feed over different Pt catalysts are summarized in Table 7. For all three catalysts, no significant hydrocracking was observed at the two (300 and 350°C) reaction temperatures studied. As observed in Table 7, Pt/ITQ-2 gives the highest aromatic reduction, especially at the lowest reaction temperature (300°C). These results further confirm the good catalytic performance obtained with the Pt/ITQ-2 catalyst in the hydrogenation of naphthalene. With respect to the aromatic distribution, the fraction of monoaromatics remained practically unchanged at 300°C reaction temperature for all three catalysts studied under the moderate hydrogen pressure used, while at 350°C most of the triaromatics and an appreciable fraction of diaromatics were converted into monoaromatics over the Pt/USY catalyst (Table 7). Taking into account that the hydrotreated LCO still has a significant amount of sulfur (400 ppm), a catalytic behavior similar to that observed in the naphthalene hydrogenation experiments in the presence of sulfur could be expected. However, what is observed is that Pt/ITQ-2 gives better results than Pt/USY in the HT-LCO hydrogenation experiments, while the opposite trend was observed for the naphthalene feed in both the absence and the presence of sulfur. This behavior can be explained by the lower accessibility and higher diffusional restrictions of the voluminous aromatic molecules present in the commercial feed in the USY zeolite as compared with the basically mesoporous structure of ITQ-2.

TABLE 7

Total Aromatic Content and Aromatic Distribution (wt%) Obtained at 300 and 350°C Reaction Temperatures in the Hydrogenation of a Hydrotreated LCO (HT-LCO) over the Different Pt-Supported Catalysts (1 wt% Pt)

		Pt/ITQ-2		Pt/USY		Pt/ASA	
	LCO-HT	300°C	350°C	300°C	350°C	300°C	350°C
Mono	24	22	21	21	33	22	22
Di	31	15	14	23	11	30	24
Tri+	12	9	5	9	1	10	8
Total aromatics	77	46	40	53	44	62	54

4. CONCLUSIONS

It has been shown that the new delaminated ITQ-2 material presents excellent properties as a support for preparing metal-supported hydrocracking and hydrogenation catalysts. In the first case, NiMo/ITQ-2 catalyst showed higher hydrocracking conversions than NiMo supported on USY zeolite and amorphous ASA and γ-alumina catalysts. Besides this high activity, NiMo/ITQ-2 displayed a low selectivity to gases and high selectivity to naphtha and middle distillates. Thus, the catalyst based on ITQ-2 combined the high activity characteristic of zeolite hydrocracking catalysts with the good selectivity toward middle distillates typical of amorphous-based catalysts.

On the other hand, Pt/USY was more active than Pt/ITQ-2 for the hydrogenation of naphthalene under mild conditions (275°C, 5.0 MPa), while the hydrogenation activity of Pt/ITQ-2 was superior to that of Pt/Al_2O_3 and Pt/ASA catalysts. Moreover, Pt/USY also presented the highest specific hydrogenation activity (activity per exposed surface Pt) and sulfur resistance during naphthalene hydrogenation. This was explained by considering that Pt atoms located in the 10 MR channels of ITQ-2 are not accessible to naphthalene molecules. In fact, Pt/ITQ-2 was seen to be ca 3.8 times more active than Pt/USY for the hydrogenation of benzene, which can diffuse through the smaller channels of the delaminated material. Moreover, when a real hydrotreated LCO feed containing ca 70 vol% aromatics, 0.4 wt% S, and 480 ppm N was used Pt/ITQ-2 produced the highest aromatic reduction at 300–350°C.

The good catalytic performance obtained in this work for ITQ-2-based catalysts for hydrocracking and hydrogenation processes involving large molecules can be related to the particular topology of the delaminated ITQ-2 material, combining a large well-defined external surface with zeolitic acidity, which favors the dispersion of the active metal phases and the bifunctional behavior of the catalyst.

ACKNOWLEDGMENTS

Financial support by the Comisión Interministerial de Ciencia y Tecnología (CICYT) of Spain is gratefully acknowledged (Project

MAT 99-0689). We are grateful to CEPSA (Spain) and Enitecnologie (Italy) for their analytical support.

REFERENCES

1. Huizinga, T., Theunissen, J. M., Minderhoud, H., and van Veen R., *Oil Gas J.*, June 26, 40 (1995).
2. Dufresne, P., Bigeard, P. H., and Billon, A., *Catal. Today* **1**, 367 (1987).
3. Scherzer, J., and Gruia, A. J., *in* "Hydrocracking Science and Technology," Chap. 12, p. 215. Dekker, New York, 1996.
4. Ward, J., *Fuel Process. Technol.* **35**, 55 (1993).
5. Maxwell, I. E., *Catal. Today* **1**, 385 (1987).
6. van den Berg, J. P., Lucien, J. P., Germaine, G., and Thielemans, G. L. B., *Fuel Process. Technol.* **35**, 119 (1993).
7. Cooper, B. H., and Donnis, B. H., *Appl. Catal.* **137**, 203 (1996).
8. Stanislaus, A., and Cooper, B. H., *Catal. Rev. Sci. Eng.* **36**, 75 (1994).
9. Corma, A., Martínez., A., Martínez-Soria, V., and Montón, J. B., *J. Catal.* **101**, 143 (1995).
10. Corma, A., Martínez, A., and Martínez-Soria, V., *J. Catal.* **169**, 480 (1997).
11. Rajagopalan, K., Peters, A. W., and Edwards, G. C., *Appl. Catal.* **23**, 69 (1986).
12. Corma, A., Faraldos, M., Martínez, A., and Mifsud, A., *J. Catal.* **122**, (1990).
13. Camblor, M. A., Corma, A., Martínez, A., Martínez-Soria, V., and Valencia, S., *J. Catal.* **179**, 537 (1998).
14. Corma, A., Fornés, V., Pergher, S. B., Maesen, Th. L. M., and Buglass, J. G., *Nature* **396**, 353 (1998).
15. Corma, A., Fornés, V., Martínez-Triguero, J., and Pergher, S. B., *J. Catal.* **186**, 57 (1999).
16. Corma, A., Fornés, V., and Pergher, S. B., Patent 9605004EP, 1996, and WO 9717290, 1997.
17. Corma, A., Fornés, V., Martínez, A., and Orchillés, A. V., *ACS Symp. Ser.* **368**, 542 (1988).
18. Emeis, C. A., *J. Catal.* **141**, 347 (1993).
19. Cid, R., Gil Llambías, F. J., González, M., and López Agudo, A., *Catal. Lett.* **24**, 147 (1994).
20. Cid, R., Orellana, F., and López Agudo, A., *Appl. Catal.* **23**, 327 (1987).
21. Corma, A., Vazquez, M. I., Bianconi, A., Clozza, A., García, J., Pallota, O., and Cruz, J. M., *Zeolites* **8**, 464 (1988).
22. Boudart, M., Ryoo, R., Valença, G. P., and van Grieken, R., *Catal. Lett.* **17**, 273 (1993).
23. Dalla-Betta, R. A., and Boudart, M., *in* "Proceedings 5th International Congress on Catalysis," p. 1329. North-Holland, Amsterdam, 1973.
24. Faye, P., and Bougeard, R. P., *Stud. Surf. Sci. Catal.* **106**, 281 (1997).
25. Henker, M., and Wedlandt, K.-P., *Appl. Catal.* **69**, 205 (1991).
26. Topsoe, H., Clausen, B. J., Topsoe, N. Y., and Pedersen, E., *Ind. Eng. Chem. Fundam.* **25**, 25 (1986).
27. Minderhoud, J. K., and van Veen, J. A. R., *Fuel Process. Technol.* **35**, 87 (1993).
28. Topsoe, N.-Y., and Topsoe, H., *J. Catal.* **139**, 641 (1993).
29. Frye, C. G., and Weitkamp, A. W., *J. Chem. Eng. Data* **14**, 372 (1969).
30. Sachtler, W. M. H., and Stakheev, A. Y., *Catal. Today* **12**, 283 (1992).
31. Lin, S. D., and Vannice, M. A., *J. Catal.* **143**, 539 (1993).
32. Lin, S. D., and Vannice, M. A., *J. Catal.* **143**, 554 (1993).
33. Chou, P., and Vannice, M. A., *J. Catal.* **107**, 129 (1987).
34. Chou, P., and Vannice, M. A., *J. Catal.* **107**, 140 (1987).
35. Gallezot, P., Datka, J., Massardier, J., Primet, M., and Imelik, B., *in* "Proceedings 6th International Congress on Catalysis," p. 696. Chem. Soc., London, 1977.
36. Homeyer, S. T., Karpinski, Z., and Sachtler, W. M. H., *J. Catal.* **123**, 60 (1990).
37. Kokayeff, P., *in* "Catalyst Hydroprocessing of Petroleum and Distillates," p. 253. Dekker, New York, 1994.
38. Huang, T. C., and Kang, B. C., *Ind. Eng. Chem. Res.* **35**, 1140 (1995).
39. Gallezot, P., *Catal. Rev. Sci. Eng.* **20**, 359 (1971).
40. Homeyer, S. T., and Sachtler, W. M. H., *Stud. Surf. Sci. Catal.* **49**, 975 (1989).
41. Dalla Betta, R. A., Boudart, M., Gallezot, P., and Weber, R. S., *J. Catal.* **69**, 514 (1981).